Optical properties of GaS-$Ca(OH)_2$ bilayer heterostructure

E. Torun,* H. Sahin, and F. M. Peeters
Department of Physics, University of Antwerp, Groenenborgerlaan 171, B-2020 Antwerp, Belgium
(Received 9 December 2015; revised manuscript received 20 January 2016; published 5 February 2016)

Finding novel atomically thin heterostructures and understanding their characteristic properties are critical for developing better nanoscale optoelectronic devices. In this study, we investigate the electronic and optical properties of a GaS-$Ca(OH)_2$ heterostructure using first-principle calculations. The band gap of the GaS-$Ca(OH)_2$ heterostructure is significantly reduced when compared to those of the isolated constituent layers. Our calculations show that the GaS-$Ca(OH)_2$ heterostructure is a type-II heterojunction which can be used to separate photoinduced charge carriers where electrons are localized in GaS and holes in the $Ca(OH)_2$ layer. This leads to spatially indirect excitons which are important for solar energy and optoelectronic applications due to their long lifetime. By solving the Bethe-Salpeter equation on top of a single shot *GW* calculation (G_0W_0), the dielectric function and optical oscillator strength of the constituent monolayers and the heterostructure are obtained. The oscillator strength of the optical transition for the GaS monolayer is an order of magnitude larger than the $Ca(OH)_2$ monolayer. We also found that the calculated optical spectra of different stacking types of the heterostructure show dissimilarities, although their electronic structures are rather similar. This prediction can be used to determine the stacking type of ultrathin heterostructures.

DOI: 10.1103/PhysRevB.93.075111

I. INTRODUCTION

The successful synthesis of graphene was a milestone in condensed matter physics and materials science [1–3]. Due to this remarkable achievement, a new field of quasi-two-dimensional (2D) materials has emerged which have changed the perspective of materials research. Since then, the attention of materials science and condensed matter physics has been widened towards new single layer structures, such as silicene [4,5], germanene [5–7], transition-metal dichalcogenides (TMDs) [8–11], alkaline-earth-metal hydroxide (AEMHs) [12], and post-transition metal chalcogenides (PTMCs) [13–15].

These individual monolayers possess various significant electronic and optical properties which make them promising candidates for the next generation of nanoscale devices [16–18]. For instance, monolayer TMDs are direct band gap semiconductors, unlike their bulk counterparts [9–11], and exhibit large exciton binding energies in the order of 0.1–1.0 eV, which results in exciton resonances at room temperature [19–22]. In addition, having strong coupling between the spin and the valley degrees of freedom opens up the possibility of valleytronic devices [23–25].

In spite of the large amount of research on graphenelike structures and ultrathin TMDs, studies on single layer AEMHs [i.e., $Ca(OH)_2$ and $Ni(OH)_2$ and PTMCs (i.e., GaS and GaSe) are sparse and have only started very recently. In the recent study of Aierken *et al.* it was shown that $Ca(OH)_2$ can be isolated in monolayer form and it is a direct band gap semiconductor independent of the number of layers [12]. Similar to $Ca(OH)_2$, monolayer GaS and GaSe have been synthesized recently and it has been shown that both monolayers are indirect gap semiconductors, and they are suitable candidates for use in field-effect transistors and nanophotonic devices [14,26–28].

Another important aspect of the mentioned layered structures is their usage as building blocks for novel multilayer heterostructures. Recently, a new field of research in materials science has emerged that deals with the stacking of two or more different monolayers on top of each other, namely, van der Waals (vdW) heterostructures [29]. This widens considerably the diversity of possibilities for new functionalities and increases the range of different electronic and optoelectronic applications. For instance, it has been shown that a *p-n* junction based on the hexagonal boron nitride (hBN)-WSe_2 heterostructure exhibits tunable electroluminescence [30]. In addition, TMD heterostructures show a tunable photovoltaic effect [31] and can be used as tunnel diodes and transistors [32]. Long-lived interlayer excitons were observed by photoluminescence excitation spectroscopy in $MoSe_2$-WSe_2 heterostructures where electrons and holes are localized in different layers [33]. It has been shown that spatially indirect excitons can also be found in MoS_2-WSe_2 heterostructures, which are type-II heterojunctions [34]. Very recently, Calman *et al.* showed that the excitons in MoS_2 and hBN vdW heterostructures can be controlled by a gate voltage, temperature, and the intensity and the helicity of the optical excitation [35].

So far, the building blocks of these multilayer heterostructures have been usually graphene (and graphenelike monolayers) or TMD monolayers, whereas in this work we propose a heterostructure whose building blocks are GaS and $Ca(OH)_2$, which are relatively new 2D crystals and they are members of PTMCs and AEMHs, respectively. We show that the GaS and $Ca(OH)_2$ monolayers have similar lattice parameters and they are wide band gap semiconductors. When they are stacked on top of each other, they form a type-II heterojunction which has a smaller band gap than the constituent layers. The calculated optical oscillator strength of the GaS monolayer is $\sim$10 times larger than the one for monolayer $Ca(OH)_2$.

This paper is organized as follows: We first provide the computational methodology in Sec. II. Then, we investigate the geometric, electronic, and optical properties of the isolated

*engin.torun@uantwerpen.be

GaS and $Ca(OH)_2$ monolayers in Sec. III and the GaS-$Ca(OH)_2$ heterostructure in Sec. IV. In Sec. V, we show that the optical spectra of the heterostructure can be used to characterize their stacking type. Finally, we conclude our results in Sec. VI.

II. COMPUTATIONAL METHODOLOGY

First-principle calculations are performed using the frozen-core projector augmented wave (PAW) [36] potentials as implemented in the Vienna *ab initio* simulation package (VASP) [37]. The electronic exchange-correlation potential is treated within the generalized gradient approximation (GGA) of Perdew-Burke-Ernzerhof (PBE) [38]. A plane-wave basis set with a kinetic energy cutoff of 500 eV is used. A vacuum spacing of more than 12 Å is taken to prevent interactions between adjacent images. A set of $20\times20\times1$ Γ centered **k**-point samplings are used for the primitive unit cells. The convergence criterion for energy is set to 10^{-5} eV between two consecutive steps in the self-consistent field calculations. The atomic positions are relaxed until the Hellmann-Feynman forces are less than 10^{-4} eV/Å. Pressures on the lattice unit cell are decreased to values less than 1.0 kbar in all directions. Atomic charge transfers are calculated using Bader's charge analysis [39]. We used the DFT-D2 method of Grimme as implemented in VASP for the van der Waals correction in all the calculations [40].

The dielectric function and the optical oscillator strength of the individual monolayers and the heterostructure are calculated by solving the Bethe-Salpeter equation (BSE) on top of the single shot GW (G_0W_0) calculation, which is performed on top of standard density functional theory (DFT) calculations including spin-orbit coupling (SOC). During this process we used a $6\times6\times1$ Γ centered **k**-point sampling. The cutoff for the response function was set to 200 eV. The number of bands used in our calculation is 320. The cutoff energy for the plane waves was chosen to be 400 eV. We include four valence and four conduction bands into the calculations in the BSE step.

Once the dielectric function is obtained, other linear optical spectral quantities such as layer dependent optical absorbance $[A(\omega)]$, transmittance $[T(\omega)]$, and frequency dependent reflectivity at normal incidence $[R(\omega)]$ can be calculated using the formulas

$$\begin{aligned} A(\omega) &= \frac{\omega}{c} L \,\mathrm{Im}\,\varepsilon(\omega), \\ T(\omega) &= 1 - A(\omega), \\ R(\omega) &= \left|\frac{\sqrt{\varepsilon(\omega)} - 1}{\sqrt{\varepsilon(\omega)} + 1}\right|^2, \end{aligned} \tag{1}$$

where c, L, ω, and $\varepsilon(\omega)$ are the speed of light, the length of the cell in the layer-normal direction, the frequency of light, and the complex dielectric function, respectively.

III. GaS AND $Ca(OH)_2$ MONOLAYERS

The optimized atomic structures of single layers of GaS and $Ca(OH)_2$ are shown in Fig. 1. The optimized lattice parameters for isolated monolayers are almost equal to each other, 3.58 and 3.59 Å for GaS and $Ca(OH)_2$, respectively. In the GaS monolayer, every Ga atom is covalently bonded to three S atoms and one Ga atom, which creates a trigonal prismatic

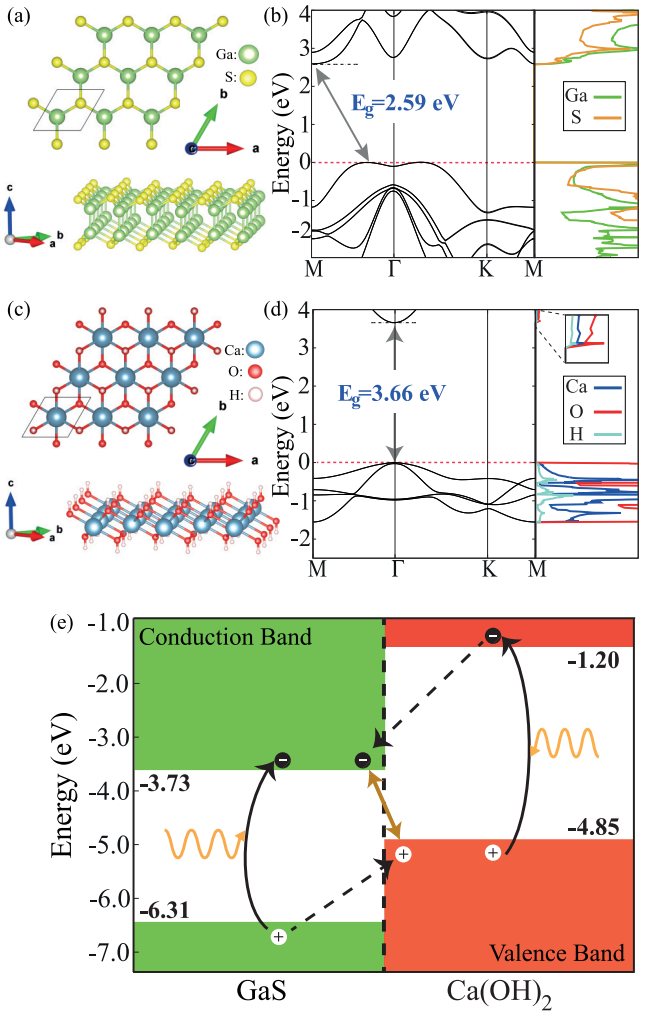

FIG. 1. The optimized atomic structures of (a) GaS and (c) $Ca(OH)_2$ monolayers and their electronic structures and PDOS (right panel) with SOC (b) and (d), respectively. The gallium, sulfur, calcium, oxygen, and hydrogen atoms are shown in green, yellow, blue, red, and white, respectively. (e) The calculated band alignment of the monolayers where the vacuum level of both materials is set to 0 eV. The red-dashed lines correspond to the Fermi level.

symmetry. The distance between two nearest neighbor Ga atoms is 2.44 Å and the Ga-S distance, 2.36 Å, is slightly shorter. In the $Ca(OH)_2$ monolayer, the Ca atom has six ionic bonds with O atoms with a bond length of 2.36 Å. Each O atom in the primitive cell has one bond with a H atom with a bond length of 0.96 Å.

The band structures including SOC of the individual monolayers are shown in Fig. 1. Both electronic structures are basically similar to the ones reported earlier [12,13]. The GaS monolayer is an indirect band gap semiconductor with a gap of 2.59 eV, as seen in Fig. 1(b). The valence band minimum (VBM) of the compound resides along the M-Γ direction, but the conduction band minimum (CBM) is at the M point in the Brillouin zone (BZ). The states in the vicinity of the Fermi level are composed of p orbitals, however, the VBM is mostly made up of the s orbitals of the Ga and S atoms. Our Bader analysis showed that the Ga-S bonds have mostly a covalent

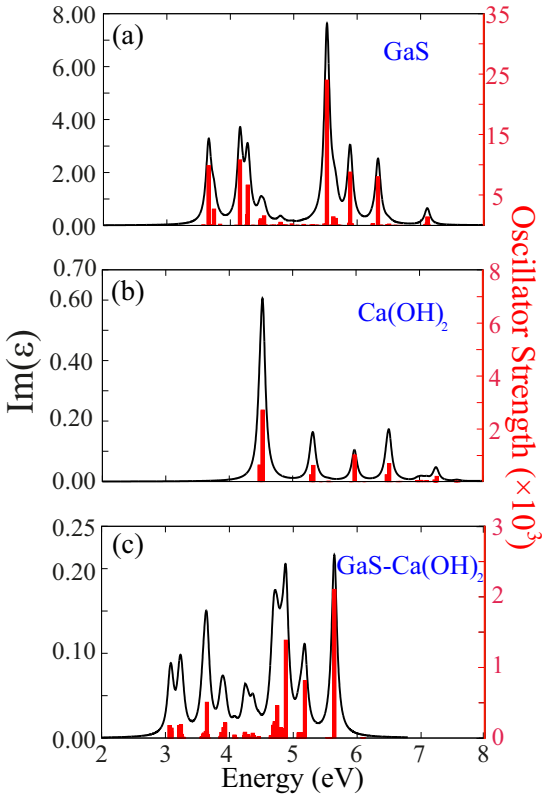

FIG. 2. Imaginary part of the dielectric function and the oscillator strength of the optical transitions of the (a) GaS monolayer, (b) Ca(OH)$_2$ monolayer, and (c) GaS-Ca(OH)$_2$ heterostructure.

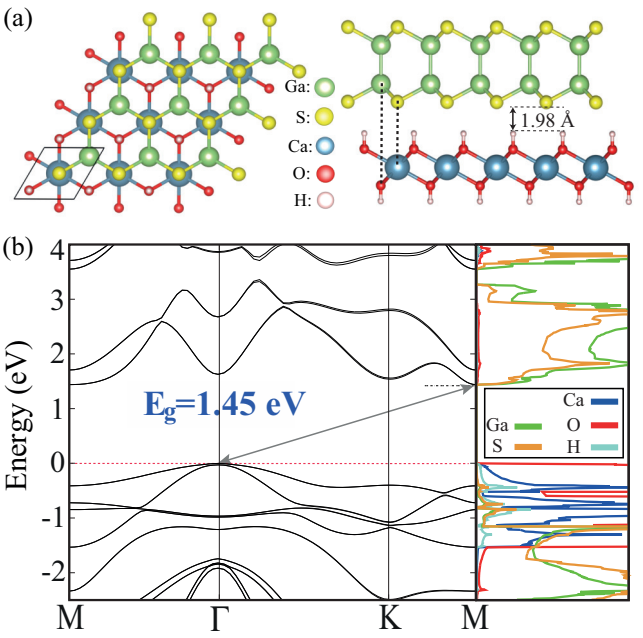

FIG. 3. (a) The optimized atomic structures of the GaS-Ca(OH)$_2$ heterostructure and (b) its electronic band structures together with the PDOS (right panel) with SOC. The gallium, sulfur, calcium, oxygen, and hydrogen atoms are shown in green, yellow, blue, red, and white, respectively. The red-dashed line corresponds to the Fermi level.

character and the Ga atoms donate 0.7e whereas each S atom gains 0.7e charge.

Contrary to the GaS monolayer, the Ca(OH)$_2$ monolayer is a direct band gap semiconductor with a band gap of 3.66 eV. The VBM and CBM of the compound are located at the Γ point in the BZ. The states at the vicinity of the Fermi level originate from the p_x and p_y orbitals of the O atom, however, the VBM is mostly from the s and p_z orbitals of the Ca and O atoms. The Ca atom and H atoms donate 1.6e and 0.6e charge, respectively, and each O atom receives 1.3e. The bonds in Ca(OH)$_2$ have mostly an ionic character.

Our calculation revealed that the vacuum levels of the isolated monolayers are different from each other. When the vacuum level of the monolayers is set to 0 eV, as shown in Fig. 1(e), the obtained heterostructure is a type-II heterojunction, which opens up the possibility of using it as an electron-hole separator under photoexcitation. As shown in the figure, the excited electrons and the holes pile up in the GaS and Ca(OH)$_2$ monolayer, respectively. Since the electrons and the holes of the heterostructure reside in different layers, the created excitons are spatially indirect and the recombination occurs through the staggered gap of the heterojuction. It has been shown that spatially indirect excitons in MX_2 heterobilayers have a long lifetime (∼20–30 ns at room temperature), which is important for applications in optoelectronics and photovoltaics [41].

In Figs. 2(a) and 2(b) the dielectric function and the oscillator strength of the optical transitions of isolated GaS and Ca(OH)$_2$ monolayers are shown, respectively. For GaS, the first peak of the dielectric function is composed of four optical transitions which are from the valence band edge to conduction band edges at the M, Γ, and K points in the Brillouin zone (BZ), which are very close in energy. For the Ca(OH)$_2$ monolayer, the first peak is composed of two optical transitions from Γ to Γ in the BZ. These two peaks are split by about 40 meV due to the SOC. The first peak of the dielectric function is considered as the optical band gap of the compound, which is at ∼3.60 and ∼4.48 eV for GaS and Ca(OH)$_2$, respectively, with an exciton binding energy of 1.12 and 2.10 eV, respectively.

IV. HETEROSTRUCTURE

Having similar lattice constants opens up the possibility of using these monolayers as the building blocks of vdW heterostructures. For this purpose, we place the GaS monolayer on top of the Ca(OH)$_2$ monolayer. In order to find the minimum energy configuration of the heterostructure, we shift the GaS monolayer along three different directions. The minimum energy configuration is obtained when the Ga and S atoms are on top of the O (and H) and Ca atom of the Ca(OH)$_2$ monolayer, respectively, as shown in Fig. 3. The geometric structure of the constituent layers of the heterostructure does not change when compared with their isolated form. The distance between the two layers is 1.98 Å and the binding energy (E_B) of the heterostructure is 0.12 eV per unit cell (Table I).

Although the interaction between these two layers is weak, there is a significant decrease in the band gap when these two single layers are stacked on top of each other [see Fig. 3(b)].

TABLE I. Ground state properties of GaS and $Ca(OH)_2$ monolayers and the heterostructure composed of these two monolayers. Calculated lattice parameters a and b, interlayer binding energy E_B (per unit cell), the band gap E_g, and the work function Φ [for the heterostructure, the first value is for the GaS and the second one is for the $Ca(OH)_2$ side, respectively] of the structures.

	$a = b$ (Å)	E_B (eV)	E_{coh}/atom (eV)	E_g (eV)	Φ (eV)
GaS	3.58		3.83	2.59(i)	6.31
$Ca(OH)_2$	3.59		4.59	3.66(d)	4.85
GaS-$Ca(OH)_2$	3.58	0.12	4.26	1.45(i)	6.21, 5.06

This dramatic modification in the band gap is due to the difference in the vacuum level of the constituent monolayers. Our calculations show that the heterostructure has an indirect band gap of 1.45 eV where the VBM is at the Γ and the CBM is at the M point in the BZ. The Γ to Γ gap is 1.63 eV. The advantage of having an indirect band gap heterostructure is that it results in long-lived excitons due to the small overlap of the electron-hole wave functions. This opens up the possibility of using the GaS-$Ca(OH)_2$ heterojunction for excitonic solar cells so that the electron-hole pairs can be split relatively easy.

As shown in Table I, the calculated work function of the heterostructure is found to be 6.21 and 5.06 eV for the GaS and $Ca(OH)_2$ sides of the heterojunction. Due to the interaction between the two layers, the work-function values diminished 0.1 and increased 0.21 eV compared with the values for the isolated GaS and $Ca(OH)_2$ monolayers, respectively.

The partial density of states (PDOS) of the GaS-$Ca(OH)_2$ heterostructure is shown in the right panel of Fig. 3(b). As expected from the band alignment, the valence band and the conduction band of the heterostructure are from the GaS and $Ca(OH)_2$ monolayers, respectively. The resulting band structure of the heterostructure is shown in Fig. 3(b). As seen, the band structure of the heterostructure is almost an overlap of the band structures of the isolated monolayers. This is due to the weak interaction between layers so that the dispersion of the bands does not change.

In order to investigate only the spatially indirect excitons in the heterostructure, four valence and four conduction bands were taken into account for the optical transitions in the BSE step. So, the optical transitions between these bands correspond to the interlayer recombination of the electrons and holes through the staggered gap. This means that the exciton peaks shown in Fig. 2(c) correspond only to spatially indirect excitons in the heterojunction. Consistent with the prediction of the gap closing in the heterostructure, the first peak in the dielectric function appears at a lower energy (∼3.10 eV) than the one of the constituent monolayers, as seen in the figure. The exciton binding energy of the heterostructure is calculated to be 0.90 eV.

Our calculations also reveal that the oscillator strengths of the GaS monolayer are an order of magnitude larger than those of the $Ca(OH)_2$ monolayer and the GaS-$Ca(OH)_2$ heterostructure. However, the oscillator strength and the dielectric function of the heterostructure resemble the properties of $Ca(OH)_2$. Similarly, as shown by Fang *et al.* [34], in the case

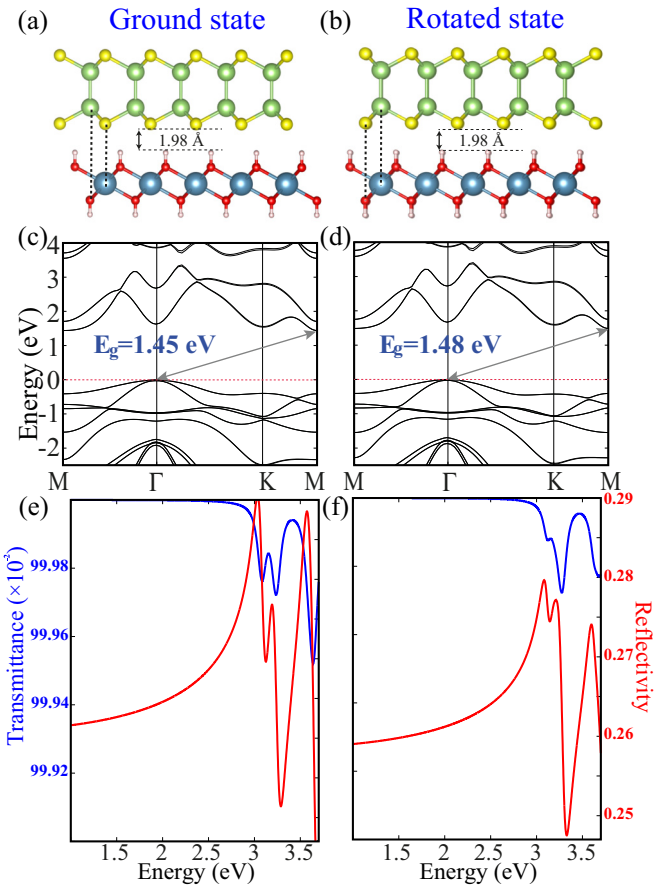

FIG. 4. The optimized atomic structures of the two lowest energy configurations of the GaS-$Ca(OH)_2$ heterostructure: (a) Ground and (b) rotated state, which has 5 meV higher energy. Their electronic structure [(c) and (d)] and optical transmittance and reflectivity [(e) and (f)]. The red-dashed lines correspond to the Fermi level.

of the MoS_2-WSe_2 heterostructure, which is also a type-II heterojunction, its optical properties resemble the ones of MoS_2. The creation of such nanoscale type-II heterojuctions leads to the formation of spatially indirect excitons, which are vital elements for exciton solar cells and optoelectronics devices due to the relatively longer lifetimes of the excitons.

V. OPTICAL CHARACTERIZATION OF STACKING TYPE

In this section, we will show that the optical spectra of ultrathin heterostructures can be used to determine their stacking type. In Fig. 4, the optimized atomic configuration, the electronic structure, and the optical transmittance and the reflectivity of the two lowest energy configurations of the GaS-$Ca(OH)_2$ heterostructure are shown. The atomic structures of these two lowest energy configurations are completely different from each other, although the energy difference between them is quite small, ∼5 meV.

The higher energy state [Fig. 4(b)] is obtained by a 180° rotation of the ground state configuration [Fig. 4(a)], so it will be referred to as the "rotated state" from now on. In the rotated state the Ga and S atoms are on top of the Ca and O (and H) atoms of the $Ca(OH)_2$ monolayer, respectively and in both cases the interlayer spacing is found to be 1.98 Å. As shown in

Figs. 4(c) and 4(d), the electronic structures of the ground and the rotated state are similar and the dispersions of the bands are identical. The only difference is that the band gap of the rotated state is 3 meV larger.

Although the electronic structures of the ground and rotated states are very close to each other, the optical transmittance and the reflectivity profiles of their band edges are distinct, as shown in Figs. 4(e) and 4(f). The main differences in the optical spectra of these two stacking cases originate from the different strengths of the optical transitions. It is predicted that the energies of these optical transitions are similar but their intensities are distinct. This is due to the different orientations of the atoms in these two stackings. For instance, the two peaks derived from the band edges are unique for both structures. As seen in the optical transmittance profile of the ground state [Fig. 4(e)], these two peaks can be easily identified because of their almost equal oscillator strength. In the rotated case, however, the oscillator strength of the first peak is much smaller than the second one, so that it cannot be identified in the transmittance profile. On the other hand, the relative intensity of the first two peaks in the reflectivity profile is also unique for each stacking case.

This prediction is rather crucial to determine the stacking types of the heterostructures in experiments. The heterojunctions which are produced by the growth technique might contain more than one stacking type, if the energy difference between the different stacking types is small. Therefore, it is important to find a powerful and sensitive tool to identify different stacking types in the produced heterostructures. In light of the above discussion, we suggest that the optical spectra (i.e., transmittance and reflectivity) can be used to identify different stacking types in a heterostructure.

VI. CONCLUSIONS

We proposed a heterostructure in which the constituent monolayers are GaS and $Ca(OH)_2$, which have been recently synthesized. These two monolayers have similar lattice constants and they are wide band gap semiconductors. When they are stacked on top of each other, the electronic band gap of the obtained heterostructure decreases significantly. Our calculations revealed that the obtained heterojunction is a type-II semiconductor in which the conduction band and the valence band are from GaS and $Ca(OH)_2$, respectively. This leads to localization of the electrons and holes in different layers, which results in spatially indirect excitons. Our BSE-G_0W_0 calculations showed that the optical oscillator strength of the GaS monolayer is an order of magnitude larger than the one of monolayer $Ca(OH)_2$. We found that the band edge profiles of the optical spectrum of different stacking types of the heterojunction show differences, although their electronic structures are rather similar. This prediction opens up the possibility of using the optical spectrum for the characterization of the stacking type of ultrathin heterostructures.

ACKNOWLEDGMENTS

This work was supported by the Flemish Science Foundation (FWO-Vl) and the Methusalem Foundation of the Flemish government. Computational resources were provided by TUBITAK ULAKBIM, High Performance and Grid Computing Center (TR-Grid e-Infrastructure), and HPC infrastructure of the University of Antwerp (CalcUA), a division of the Flemish Supercomputer Center (VSC), which is funded by the Hercules foundation. H.S. is supported by a FWO Pegasus long Marie Curie Fellowship.

[1] K. S. Novoselov, A. K. Geim, S. V. Morozov, D. Jiang, Y. Zhang, S. V. Dubonos, I. V. Grigorieva, and A. A. Firsov, Science **306**, 666 (2004).
[2] K. S. Novoselov, D. Jiang, F. Schedin, T. J. Booth, V. V. Khotkevich, S. V. Morozov, and A. K. Geim, Proc. Natl. Acad. Sci. USA **102**, 10451 (2005).
[3] A. K. Geim and K. S. Novoselov, Nat. Mater. **6**, 183 (2007).
[4] G. G. Guzmàn-Verri and L. C. Lew Yan Voon, Phys. Rev. B **76**, 075131 (2007).
[5] S. Cahangirov, M. Topsakal, E. Akturk, H. Sahin, and S. Ciraci, Phys. Rev. Lett. **102**, 236804 (2009).
[6] M. Houssa, G. Pourtois, V. V. Afanasév, and A. Stesmans, Appl. Phys. Lett. **96**, 082111 (2010).
[7] H. Sahin, S. Cahangirov, M. Topsakal, E. Bekaroglu, E. Akturk, R. T. Senger, and S. Ciraci, Phys. Rev. B **80**, 155453 (2009).
[8] A. H. C. Neto and K. Novoselov, Rep. Prog. Phys. **74**, 082501 (2011).
[9] K. F. Mak, C. Lee, J. Hone, J. Shan, and T. F. Heinz, Phys. Rev. Lett. **105**, 136805 (2010).
[10] A. Splendiani, L. Sun, Y. Zhang, T. Li, J. Kim, C.-Y. Chim, G. Galli, and F. Wang, Nano Lett. **10**, 1271 (2010).
[11] Q. H. Wang, K. Kalantar-Zadeh, A. Kis, J. N. Coleman, and M. S. Strano, Nat. Nanotechnol. **7**, 699 (2012).
[12] Y. Aierken, H. Sahin, F. Iyikanat, S. Horzum, A. Suslu, B. Chen, R. T. Senger, S. Tongay, and F. M. Peeters, Phys. Rev. B **91**, 245413 (2015).
[13] Y. Ma, Y. Dai, M. Guo, L. Yu, and B. Huang, Phys. Chem. Chem. Phys. **15**, 7098 (2013).
[14] X. Meng, A. Pant, H. Cai, J. Kang, H. Sahin, B. Chen, K. Wu, S. Yang, A. Suslu, F. M. Peeters, and S. Tongay, Nanoscale **7**, 17109 (2015).
[15] T. Cao, Z. Li, and S. G. Louie, Phys. Rev. Lett. **114**, 236602 (2015).
[16] C. Ataca, H. Sahin, and S. Ciraci, J. Phys. Chem. C **116**, 8983 (2012).
[17] P. Miró, M. Audiffred, and T. Heine, Chem. Soc. Rev. **43**, 6537 (2014).
[18] M. Chhowalla, H. S. Shin, H. S. Shin, L.-J. Li, K. P. Loh, and H. Zhang, Nat. Chem. **5**, 263 (2013).
[19] K. He, N. Kumar, L. Zhao, Z. Wang, K. F. Mak, H. Zhao, and J. Shan, Phys. Rev. Lett. **113**, 026803 (2014).
[20] A. R. Klots, A. K. M. Newaz, B. Wang, D. Prasai, H. Krzyzanowska, J. Lin, D. Caudel, N. J. Ghimire, J. Yan, B. L. Ivanov, K. A. Velizhanin, A. Burger, D. G. Mandrus, N. H. Tolk, S. T. Pantelides, and K. I. Bolotin, Sci. Rep. **4**, 6608 (2014).

[21] A. Chernikov, T. C. Berkelbach, H. M. Hill, A. Rigosi, Y. Li, O. B. Aslan, D. R. Reichman, M. S. Hybertsen, and T. F. Heinz, Phys. Rev. Lett. **113**, 076802 (2014).
[22] M. M. Ugeda, A. J. Bradley, S.-F. Shi, F. H. da Jornada, Y. Zhang, D. Y. Qiu, W. Ruan, S.-K. Mo, Z. Hussain, Z.-X. Shen, F. Wang, S. G. Louie, and M. F. Crommie, Nat. Mater. **13**, 1091 (2014).
[23] K. F. Mak, K. He, J. Shan, and T. F. Heinz, Nat. Nanotechnol. **7**, 494 (2012).
[24] G. Sallen, L. Bouet, X. Marie, G. Wang, C. R. Zhu, W. P. Han, Y. Lu, P. H. Tan, T. Amand, B. L. Liu, and B. Urbaszek, Phys. Rev. B **86**, 081301(R) (2012).
[25] X. Xu, W. Yao, D. Xiao, and T. F. Heinz, Nat. Phys. **10**, 343 (2014).
[26] D. J. Late, B. Liu, H. S. S. R. Matte, C. N. R. Rao, and V. P. Dravid, Adv. Funct. Mater. **22**, 1894 (2012).
[27] D. J. Late, B. Liu, J. Luo, A. Yan, H. S. S. R. Matte, M. Grayson, C. N. R. Rao, and V. P. Dravid, Adv. Funct. Mater. **24**, 3549 (2012).
[28] P. A. Hu, Z. Z. Wen, L. F. Wang, P. H. Tan, and K. Xiao, ACS Nano **6**, 5988 (2012).
[29] A. K. Geim and I. V. Grigorieva, Nature (London) **499**, 419 (2013).
[30] J. S. Ross, P. Klement, A. M. Jones, N. J. Ghimire, J. Yan, D. G. Mandrus, T. Taniguchi, K. Watanabe, K. Kitamura, W. Yao, D. H. Cobden, and X. Xu, Nat. Nanotechnol. **79**, 268 (2014).
[31] M. M. Furchi, A. Pospischil, F. Libisch, J. Burgdörfer, and T. Mueller, Nano Lett. **14**, 4785 (2014).
[32] T. Roy, M. Tosun, X. Cao, H. Fang, D.-H. Lien, P. Zhao, Y.-Z. Chen, Y.-L. Chueh, J. Guo, and A. Javey, ACS Nano **9**, 2071 (2015).
[33] P. Rivera, J. R. Schaibley, A. M. Jones, J. S. Ross, S. Wu, G. Aivazian, P. Klement, K. Seyler, G. Clark, N. J. Ghimire, J. Yan, D. G. Mandrus, W. Yao, and X. Xu, Nat. Commun. **6**, 6242 (2015).
[34] H. Fang, C. Battaglia, C. Carraro, S. Nemsak, B. Ozdol, J. S. Kang, H. A. Bechtel, S. B. Desai, F. Kronast, A. A. Unal, G. Conti, C. Conlon, G. K. Palsson, M. C. Martin, A. M. Minor, C. S. Fadley, E. Yablonovitch, R. Maboudian, and A. Javey, Proc. Natl. Acad. Sci. USA **111**, 6198 (2014).
[35] E. V. Calman, C. J. Dorow, M. M. Fogler, L. V. Butov, S. Hu, A. Mishchenko, and A. K. Geim, arXiv:1510.04410.
[36] G. Kresse and D. Joubert, Phys. Rev. B **59**, 1758 (1999).
[37] G. Kresse and J. Hafner, Phys. Rev. B **47**, 558(R) (1993).
[38] J. P. Perdew, K. Burke, and M. Ernzerhof, Phys. Rev. Lett. **77**, 3865 (1996).
[39] R. F. W. Bader, *Atoms in Molecules—A Quantum Theory* (Oxford University Press, Oxford, UK, 1990).
[40] S. Grimme, J. Comput. Chem. **27**, 1787 (2006).
[41] M. Palummo, M. Bernardi, and J. C. Grossman, Nano Lett. **15**, 2794 (2015).